Vibration analysis of piezoelectric laminated slightly curved beams using distributed transfer function method

Ken Susanto *

Dept. of Mechanical Engineering, University of Southern California, Los Angeles, CA 90089-1453, United States

ARTICLE INFO

ABSTRACT

Piezoelectric laminated slightly curved beams (PLSCB) is currently one of the most popular actuators used in smart structure applications due to the fact that these actuators are small, lightweight, quick response and relatively high force output. This paper presents an analytical model of PLSCB, which includes the computation of natural frequencies, mode shapes and transfer function formulation using the distributed transfer function method (DTFM). By setting the radius of curvature of the proposed model to infinity, a piezoelectric laminated straight beams (PLSB) model can be obtained. The DTFM is applied and extended to carry out the transfer function formulation of the PLSCB and PLSB models. This method will be used to solve for the natural frequencies, mode shapes and transfer functions of the PLSCB and PLSB models in exact and closed form solution without using truncated series of particular comparison or admissible functions. The natural frequencies of the cantilevered PLSCB and PLSB are calculated by the DTFM and the Rayleigh–Ritz method. The analysis indicates that the stretching–bending coupling due to curvature has a considerable effect on the frequency parameters. Increasing the radius of curvature of the PLSCB has its largest effect on the natural frequencies. But the inhomogeneity of the boundary conditions does not have any effects on the natural frequencies or system spectrum due to the both receptance and boundary transfer functions have the same characteristic equations. The method can also be generalized to the vibration analysis of non-piezoelectric composite beams with arbitrary boundary conditions.

© 2008 Elsevier Ltd. All rights reserved.

1. Introduction

Rapid developments in intelligent biomedical devices using piezoelectric laminated slightly curved beams (PLSCB) actuators have been proposed, which include a piezoelectric cell stretching device (Clark et al., 2000), a stimulator for cultured bone cells (Tanaka, 1999), a device for straining flexible cell culture membranes (Schaffer et al., 1994) and a novel piezoelectric forceps actuator for minimum invasive surgery (Susanto and Yang, 2004; Susanto and Yang, 2007; Susanto, 2008). Furthermore, the piezoelectric actuators also have been used in controlling the shape of the satellite antenna (Washington, 1996; Granger et al., 2000) and damping of wings (Crawley and de Luis, 1987). Piezoelectric actuators are currently one of the most popular and widely available to be used in smart structure applications because these actuators are small, lightweight, low power requirements, respond quickly and generate relatively high force output (Damjanovic and Newnham, 1992). Several studies demonstrated the benefits of the use of mechanically pre-stressed and curved shape piezoceramics actuator, THUNDER (THin Layer Composite UNimorph Ferroelectric Drive and SEnsoR), had better performance in generating high displacement out of plane and high force output (Shakeri et al., 1999; Mossi et al., 1999; Ounaies et al., 2001; Balakrishnan and Niezrecki, 2001; Yoon et al., 2000) and C-block actuator (Moskalik and Brei, 1999) compared to standard geometrically straight piezoelectric actuator.

The vibration of curved beam is a topic that has been investigated by a number of researchers, as illustrated in Table 1. This table illustrates the breakdown of research on curved beams into different categories, with the primary division being between individual curved beams. The research on individual curved beams can be further broken down into composite curved beams, composed of a number of layers; and homogeneous curved beams, fabricated from one solid material. Finally, the research can be categorized on the basis of the assumptions made to determine the equations of motion, which range from neglecting the effects of rotatory inertia and transverse shear and assuming an inextensible neutral axis to including the effects of rotatory inertia and transverse shear and assuming an extensible neutral axis.

The body of research on individual curved beam vibration has been reviewed quite comprehensively. The latest, most complete review was by Chidamparam and Leissa (1995), including over 400 references. Other review of curved beam literatures were also done by Auciello and De Rosa (1993) and also Laura and Maurizi (1987). These reviews presented a wealth of information

* Tel.: +1 310 544 9375.
E-mail address: ksusanto@verizon.net

Table 1
Literature review of curved beams.

Homogeneous curved beams				Composite curved beams			
Non-piezoelectric				Non-piezoelectric		Piezoelectric	
Inextensional neutral axis	Extensional neutral axis	With rotatory inertia	With trans. shear	Semi circular	Slight curved	Semi circular	Slight curved
Den Hartog (1928)	Nelson (1962)	Hammoud and Archer (1963)	Buckens (1950)	Dym (1980)	Qatu (1992)	Larson and Vinson (1993)	NONE
Archer (1960)	Chidamparam and Leissa (1995)		Seidel and Erdelyi (1964)	Qatu (1993)		Washington (1996)	
Laura and Maurizi (1987)	Veletsos et al. (1972)		Rao and Sundararajan (1969)	Qatu (2004)		Mitchell et al. (1997)	
Auciello and De Rosa (1993)			Irie et al. (1983)			Moskalik and Brei (1997)	
Love (1944)							

on homogeneous curved beams, but illustrated the comparative scarcity of literature on composite curved beams. Den Hartog (1928), Archer (1960), Laura and Maurizi (1987), Auciello and De Rosa (1993) and Love (1944) examined homogenoeuos curved beams that were very thin; the assumption of inextensibility, coupled with the absence of rotatory inertia and shear deformation to solve for the natural frequencies. Nelson (1962) and Chidamparam and Leissa (1995) compared the natural frequencies generated by extensional and inextensional theory for pinned homogeneous curved beams. Veletsos et al. (1972) studied for the natural frequencies of the homogeneous thick curved beams with extensional and shear deformation effects. Hammoud and Archer (1963) examined the natural frequencies of the homogeneous thick curved beams with extensional and rotatory inertia effects. Buckens (1950), Seidel and Erdelyi (1964), Rao and Sundararajan (1969) and Irie et al. (1983) computationally determined the natural frequencies of the homogeneous curved beams which includes transverse shear effect.

Many researchers examining the dynamic behavior of composite curved beams like Dym (1980), merely derived equations of motion for the curved beam, but without a piezoelectric term. These equations of motion for composite curved beams are identical in form to those for homogeneous beams, but incorporate laminate stiffness in place of the homogeneous extensional and bending stiffness.

Qatu (1993) used these equations of motion to find the natural frequencies of specific geometries of pinned composite beams, and extended the theory with the inclusion of rotatory inertia and transverse shear to find the natural frequencies of thicker pinned composite beams. Qatu and Elsharkawy (1993) proposed Ritz method to solve for the natural frequencies of the laminated composite arches with deep curvature and arbitrary boundaries. Later, Qatu (2004) compiled a monograph research works of vibration analysis of composite shells and plates, which included the non-piezoelectric composite curved beam.

Larson and Vinson (1993) included piezoelectric term in the equations of motion of composite shells composite curved beams and rings. Although they used these equations of motion to develop solutions for the static behavior of curved composite beams, they did not investigate the dynamic behavior or its natural frequencies.

Washington (1996) added the piezoelectric term to the composite circular beams by Qatu (1993) to study the quasi-static behavior of satellite antenna. Mitchell et al. (1997) improved the composite piezoelectric circular beams model by including first order shear deformation. But, none of them determined any dynamic responses or natural frequencies of the piezoelectric composite curved beams.

Moskalik and Brei (1997) added the piezoelectric term to the derived non-piezoelectric composite circular beams model by Qatu

(1993) in order to study the static and dynamic behaviors of the C-block actuator.

However, the work of these researchers provides a useful guidance on which to base the development of the equations of motion for the PLSCB, even though additional work must be done to complete the modeling and analysis. The only non-piezoelectric laminated slightly curved beams model by Qatu (1992) can be modified and extended by adding piezoelectric term on its governing equations to derive the PLSCB model.

This paper presents an analytical model of the piezoelectric laminated slightly curved beam (PLSCB), as shown in Fig. 1, derived using the Hamilton's principle. Then, the governing equations of the PLSCB are solved using the distributed transfer function method (DTFM) (Yang and Tan, 1992). By setting the radius of curvature of the PLSCB model to infinity, a piezoelectric laminated straight beams (PLSB) model is derived, as shown in Fig. 2. The DTFM is applied and extended to carry out the transfer function formulation of the PLSCB and PLSB models. This method will be used to solve for the natural frequencies, mode shapes and transfer functions of the PLSCB and PLSB models in exact and closed form solution without using any truncated series of particular comparison or admissible functions. Furthermore, this method also does not require any eigensolution. Compared to Rayleigh–Ritz method, the DTFM has the capability of providing exact and closed-form solution for vibration analysis of the composite beams with arbitrary boundary conditions and physical insight behavior of the continuous structure.

2. PLSCB and PLSB models

The dynamic model of the PLSCB, as shown in Fig. 1, is derived using the Hamilton's principle. The thin beams are studied here where effects of shear deformation and rotatory inertia will be neglected.

The first step in determining the strain energy, which will be used in the Hamilton's principle, is to determine an expression for the stress within the curved beam. The magnitude of the stress in the circumferential direction at any point of the curved beam is given by the piezoelectric constitutive law (IEEE, 1998) as follows:

$$\sigma = Y\varepsilon = Y(\varepsilon_m + \varepsilon_p), \tag{2.1}$$

where the mechanical strain, ε_m, and piezoelectric induced strain, ε_p, (Moskalik and Brei, 1997) are defined as follows:

$$\begin{aligned} \varepsilon_m &= \varepsilon^0 + z\kappa, \\ \varepsilon_p &= d_{31}E_3(t). \end{aligned} \tag{2.2}$$

Y is Young's modulus of the material, $d_{31}E_3(t)$ is the induced piezoelectric strain, $E_3(t)$ is the applied electric field function of time through the thickness of the piezoelectric elements, ε^0 is the exten-
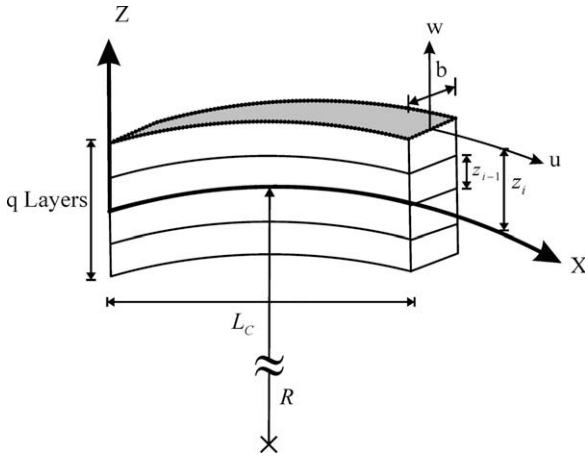
Fig. 1. Schematic drawing of piezoelectric laminated slightly curved beams (PLSCB).
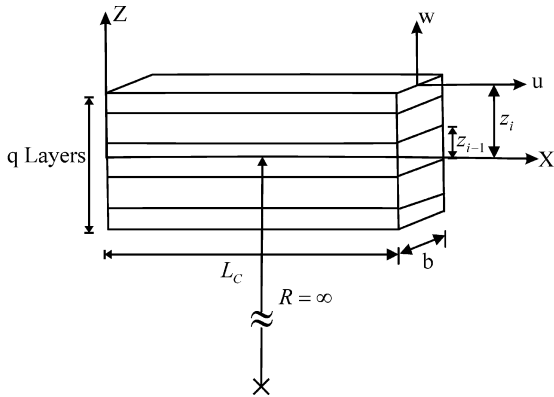

Fig. 2. Schematic drawing of piezoelectric laminated straight beams (PLSB).

sional strain at the neutral axis, z is the distance from the neutral axis and κ is the change in curvature of the neutral axis during bending. The electric field, E_3, is defined as positive if it is applied in the same direction as the polarity of the piezoelectric element and negative if applied in the opposite direction. The piezoelectric strain constant, d_{31}, relates the electric field in the radial direction to circumferential strains. In poled piezoelectric ceramics, d_{31} is a negative quantity; in non-active materials, it is assumed to be zero.

The stress of each layer of the shallow curved beam can be found by substituting Eq. (2.2) into the piezoelectric constitutive equation, Eq. (2.1) to yield

$$\sigma_i = Y_i(\varepsilon^0 + z\kappa + (d_{31}E_3(t))_i), \tag{2.3}$$

where number of layers, $i = 1, 2, \ldots, q$.

The strain and curvature at the mid-plane of the slightly curved beam are expressed in terms of circumference and radial displacements (Qatu, 1992) as follows:

$$\varepsilon^0 = \frac{\partial u(x,t)}{\partial x} + \frac{w(x,t)}{R}, \tag{2.4}$$

$$\kappa = \frac{-\partial^2 w(x,t)}{\partial x^2}, \tag{2.5}$$

where $u(x,t)$ and $w(x,t)$ represent the circumferential an radial displacement of the structure's geometrical mid-plane in the x and z directions, respectively, and R represents radius of curvature of the curved beam.

The normal force at any cross-section is defined as the stress integrated over the cross-sectional area. Due to the existence of the multi layers of the beam, as shown in Fig. 1, the integration must be performed piecewise over the cross-sectional area. Integrating the normal force, Eq. (2.3), across the q layers of the composite cross-sectional area, A, yields

$$
\begin{aligned}
N &= \int_A \sigma \, dA = b \sum_{i=1}^{q} \int_{z_{i-1}}^{z_i} Y_i(\varepsilon^0 + z\kappa + (d_{31}E_3(t))_i)dz \\
&= b \sum_{i=1}^{q} Y_i(z_i - z_{i-1})\varepsilon^0 + \frac{1}{2}b \sum_{i=1}^{q} Y_i(z_i^2 - z_{i-1}^2)\kappa \\
&\quad + b \sum_{i=1}^{q} Y_i(z_i - z_{i-1})(d_{31}E_3(t))_i,
\end{aligned}
\tag{2.6}
$$

where the subscript i refers to the ith layer, Y_i is the Young modulus of the ith layer, z_i is the distance from the neutral axis to the outside of the ith layer and b is the width.

Calculated in a similar way to the normal force, the moment about the neutral axis is defined as the stress, Eq. (2.3), multiplied by a moment arm to the neutral axis, z, and integrated over the cross-sectional area

$$
\begin{aligned}
M &= \int_A \sigma z \, dA = \sum_{i=1}^{q} b \int_{z_{i-1}}^{z_i} Y_i(\varepsilon^0 + z\kappa + (d_{31}E_3(t))_i)z\,dz \\
&= \frac{1}{2}b \sum_{i=1}^{q} Y_i(z_i^2 - z_{i-1}^2)\varepsilon^0 + \frac{1}{3}b \sum_{i=1}^{q} Y_i(z_i^3 - z_{i-1}^3)\kappa \\
&\quad + \frac{1}{2}b \sum_{i=1}^{q} Y_i(z_i^2 - z_{i-1}^2)(d_{31}E_3(t))_i.
\end{aligned}
\tag{2.7}
$$

The normal force and moment, Eqs. (2.6) and (2.7), can be restated in a matrix form as follows:

$$
\begin{Bmatrix} N \\ M \end{Bmatrix} = \begin{bmatrix} A & B \\ B & D \end{bmatrix} \begin{Bmatrix} \varepsilon^0 \\ \kappa \end{Bmatrix} + \begin{Bmatrix} N_p(t) \\ M_p(t) \end{Bmatrix}, \tag{2.8}
$$

where the constants A, B and D are the extensional, coupling and bending stiffness, respectively, and are defined as

$$A = b \sum_{i=1}^{q} Y_i(z_i - z_{i-1}), \tag{2.9a}$$

$$B = \frac{1}{2}b \sum_{i=1}^{q} Y_i(z_i^2 - z_{i-1}^2), \tag{2.9b}$$

$$D = \frac{1}{3}b \sum_{i=1}^{q} Y_i(z_i^3 - z_{i-1}^3). \tag{2.9c}$$

Likewise, the piezoelectric forcing terms N_p and M_p in Eq. (2.8) are defined as

$$N_p(t) = b \sum_{i=1}^{q} Y_i(z_i - z_{i-1})(d_{31}E_3(t))_i, \tag{2.10a}$$

$$M_p(t) = \frac{1}{2}b \sum_{i=1}^{q} Y_i(z_i^2 - z_{i-1}^2)(d_{31}E_3(t))_i, \tag{2.10b}$$

where $d_{31} = 0$ in the non-piezoelectric layers.

The strain energy of the multi-layered curved beam during the deformation can be expressed by using Eq. (2.3), as follows:

$$U = \frac{1}{2}\int_V \sigma\varepsilon \, dV = \sum_{i=1}^{q} U_i = \frac{1}{2}b \sum_{i=1}^{q} \int_0^{L_c} \int_{z_{i-1}}^{z_i} Y_i(\varepsilon^0 + z\kappa + (d_{31}E_3(t))_i)^2 dz\,dx, \tag{2.11}$$

where U is a total internal strain energy, σ is a mechanical stress, ε is a mechanical strain plus piezoelectric induced strain and V is a volume of a curved beam bonded with piezoelectric layers.

The Hamilton principle uses the variance of the energy in the system; thus, the objective is to determine the variance of the

strain energy rather than the energy itself. The variance of the strain energy shown in Eq. (2.11) is

$$\delta U = b\sum_{i=1}^{q}\int_0^{L_C}\int_{z_{i-1}}^{z_i} Y_i[(\varepsilon^0 + z\kappa + d_{31}E_3(t))\delta\varepsilon^0$$
$$+ (z\varepsilon^0 + z^2\kappa + zd_{31}E_3(t))\delta\kappa]dz\,dx$$
$$= b\sum_{i=1}^{q}\int_0^{L_C}\int_{z_{i-1}}^{z_i}(\sigma\delta\varepsilon^0 + \sigma z\delta\kappa)dz\,dx. \tag{2.12}$$

Furthermore, the variance of the strain energy, Eq. (2.12), can be expressed in terms of the normal force and moment. Using the definitions of normal force, Eq. (2.6), and moment, Eq. (2.7), the variance of the strain energy, Eq. (2.12), can be shown as follows:

$$\delta U = \int_0^{L_C}(N\delta\varepsilon^0 + M\delta\kappa)dx. \tag{2.13}$$

To produce the equations of motion, the strain energy variance equation must be restated in terms of the circumferential, u, and radial, w, displacements instead of the strain and the curvature change. Substituting the displacement relations, Eqs. (2.4) and (2.5), into the variance of the potential energy, Eq. (2.13), results in a simplified expression for the variation of the strain energy

$$\delta U = \int_0^{L_C}\left[N\delta\left(\frac{\partial u(x,t)}{\partial x}\right) + \frac{N}{R}\delta w(x,t) - M\delta\left(\frac{\partial^2 w(x,t)}{\partial x^2}\right)\right]dx. \tag{2.14}$$

Taking integration by parts of Eq. (2.14) yields

$$\delta U = \int_0^{L_C}\left[-\frac{\partial N}{\partial x}\delta u(x,t) + \frac{N}{R}\delta w(x,t) - \frac{\partial^2 M}{\partial x^2}\delta w(x,t)\right]dx$$
$$+ \left(N\delta u(x,t)\Big|_0^{L_C} + \frac{\partial M}{\partial x}\delta w(x,t)\Big|_0^{L_C} - M\delta\left(\frac{\partial w(x,t)}{\partial x}\right)\Big|_0^{L_C}\right). \tag{2.15}$$

Kinetic energy of the curved beam can be expressed as follows:

$$T = \frac{1}{2}\int_0^{L_C}\bar\rho\left[\left(\frac{\partial u(x,t)}{\partial t}\right)^2 + \left(\frac{\partial w(x,t)}{\partial t}\right)^2\right]dx, \tag{2.16}$$

where $\bar\rho = \sum_{i=1}^{q}\rho_i b_i(z_i - z_{i-1})$ is the average mass density of the beams per unit length.

The variation of the kinetic energy, Eq. (2.16) is

$$\delta T = \int_0^{L_C}\bar\rho\left[\left(\frac{\partial u(x,t)}{\partial t}\right)\delta\left(\frac{\partial u(x,t)}{\partial t}\right) + \left(\frac{\partial w(x,t)}{\partial t}\right)\delta\left(\frac{\partial w(x,t)}{\partial t}\right)\right]dx. \tag{2.17}$$

By assuming that variations and differentiations are interchangeable and the fact that $\delta u = \delta w = 0$ at $t = t_1 = t_2$, one can carry out the integration by parts of equation (2.17), which involved in the Hamilton principle as follows:

$$\int_{t_1}^{t_2}\delta T dt = \int_{t_1}^{t_2}\int_0^{L_C}\bar\rho\left[\frac{\partial u(x,t)}{\partial t}\frac{\partial}{\partial t}\delta u(x,t) + \frac{\partial w(x,t)}{\partial t}\frac{\partial}{\partial t}\delta w(x,t)\right]dx\,dt$$
$$= -\int_{t_1}^{t_2}\int_0^{L_C}\bar\rho\left[\frac{\partial^2 u(x,t)}{\partial t^2}\delta u(x,t) + \frac{\partial^2 w(x,t)}{\partial t^2}\delta w(x,t)\right]dx\,dt. \tag{2.18}$$

With the variance of the kinetic energy and potential energy defined, all quantities necessary to implement the Hamilton principle are now determined. The Hamilton principle states that the time integral of the variation of the potential strain energy, U, minus the variation of kinetic energy, T, equals zero

$$\int_{t_1}^{t_2}[\delta U - \delta T]dt = 0. \tag{2.19}$$

Substituting the variance quantities of potential energy and kinetic energy, Eqs. (2.15) and (2.18), respectively, into the Hamilton principle, Eq. (2.19) yields

$$\int_{t_1}^{t_2}\delta(U-T)dt = \int_{t_1}^{t_2}\left[\int_0^{L_C}\left[-\frac{\partial N}{\partial x}\delta u + \frac{N}{R}\delta w - \frac{\partial^2 M}{\partial x^2}\delta w + \bar\rho\frac{\partial^2 u}{\partial t^2}\delta u + \bar\rho\frac{\partial^2 w}{\partial t^2}\delta w\right]dx\right.$$
$$\left.+ N\delta u\Big|_0^{L_C} + \frac{\partial M}{\partial x}\delta w\Big|_0^{L_C} - M\delta\left(\frac{\partial w}{\partial x}\right)\Big|_0^{L_C}\right]dt = 0. \tag{2.20}$$

Based on the Hamilton principle, Eq. (2.20), the equations of motion of the PLSCB associated with its boundary conditions can be written as follows:

$$\frac{\partial N}{\partial x} = \bar\rho\frac{\partial^2 u(x,t)}{\partial t^2}, \tag{2.21a}$$
$$-\frac{N}{R} + \frac{\partial^2 M}{\partial x^2} = \bar\rho\frac{\partial^2 w(x,t)}{\partial t^2}, \tag{2.21b}$$

where

$$\frac{\partial}{\partial x}(N) = \frac{\partial}{\partial x}(A\varepsilon^o + B\kappa + N_p(t))$$
$$= \frac{\partial}{\partial x}\left(A\left(\frac{\partial u(x,t)}{\partial x} + \frac{w(x,t)}{R}\right) + B\left(-\frac{\partial^2 w(x,t)}{\partial x^2}\right)\right)$$
$$+ \underbrace{\frac{\partial}{\partial x}\left(b\sum_{i=1}^{q}Y_i(z_i - z_{i-1})(d_{31}E_3(t))_i\right)}_{0}$$

and

$$\frac{\partial^2}{\partial x^2}(M) = \frac{\partial^2}{\partial x^2}(B\varepsilon^o + D\kappa + M_p(t))$$
$$= \frac{\partial^2}{\partial x^2}\left(B\left(\frac{\partial u(x,t)}{\partial x} + \frac{w(x,t)}{R}\right) + D\left(-\frac{\partial^2 w(x,t)}{\partial x^2}\right)\right)$$
$$+ \underbrace{\frac{\partial^2}{\partial x^2}\left(\frac{1}{2}b\sum_{i=1}^{q}Y_i(z_i^2 - z_{i-1}^2)(d_{31}E_3(t))_i\right)}_{0}.$$

By assuming uniformly distributed external electric field, E_3 is a function of time and independent of space, the piezoelectric induced control force, N_p and control moment, M_p of Eq. (2.21) are equal to zero when taking partial derivative with respect to x-coordinate. After this reduction, the equations of motion of PLSCB, which will be shown in Eq. (2.22), are the same as those of non-piezoelectric slightly curved composite beams modeled by Qatu (1992) without any additional of piezoelectric force terms. However, it also should be noted that the boundary conditions of the PLSCB, which will be shown in Eq. (2.23), are different from those of non-piezoelectric slightly curved composite beams due to the additional of the boundary piezoelectric induced control force and moment terms.

The equations of motion of the cantilevered PLSCB as defined for $0 \leqslant x \leqslant L_c$ can be reinstated in terms of circumferential and radial displacements by substituting combination equations 2.4, 2.5 and 2.8 into Eq. (2.21), shown as follows:

$$A\frac{\partial^2 u(x,t)}{\partial x^2} + \frac{A}{R}\frac{\partial w(x,t)}{\partial x} - B\frac{\partial^3 w(x,t)}{\partial x^3} = \bar\rho\frac{\partial^2 u(x,t)}{\partial t^2}, \tag{2.22a}$$
$$-D\frac{\partial^4 w(x,t)}{\partial x^4} + \frac{2B}{R}\frac{\partial^2 w(x,t)}{\partial x^2} - \frac{A}{R^2}w(x,t) + B\frac{\partial^3 u(x,t)}{\partial x^3}$$
$$- \frac{A}{R}\frac{\partial u(x,t)}{\partial x} = \bar\rho\frac{\partial^2 w(x,t)}{\partial t^2} + \frac{N_p(t)}{R}. \tag{2.22b}$$

The clamped-free boundary conditions of the PLSCB ($x = 0, L_C$) can be shown as follows:

$$u|_{x=0} = 0, \quad \left[A \frac{\partial u(x,t)}{\partial x} + \frac{A}{R} w(x,t) - B \frac{\partial^2 w(x,t)}{\partial x^2} + N_p(t) \right]\bigg|_{x=L_c} = 0, \quad (2.23a)$$

$$w|_{x=0} = 0, \quad \left[B \frac{\partial^2 u(x,t)}{\partial x^2} + \frac{B}{R} \frac{\partial w(x,t)}{\partial x} - D \frac{\partial^3 w(x,t)}{\partial x^3} \right]\bigg|_{x=L_c} = 0, \quad (2.23b)$$

$$\frac{\partial w}{\partial x}\bigg|_{x=0} = 0, \quad \left[B \frac{\partial u(x,t)}{\partial x} + \frac{B}{R} w(x,t) - D \frac{\partial^2 w(x,t)}{\partial x^2} + M_p(t) \right]\bigg|_{x=L_c} = 0. \quad (2.23c)$$

By setting the radius of curvature of the PLSCB model to infinity or $R = \infty$ in Eqs. (2.22) and (2.23), the equations of motion of PLSB associated with its boundary conditions, as shown in Fig. 2, are derived as follows:

$$A \frac{\partial^2 u(x,t)}{\partial x^2} - B \frac{\partial^3 w(x,t)}{\partial x^3} = \bar{\rho} \frac{\partial^2 u(x,t)}{\partial t^2}, \quad (2.24a)$$

$$-D \frac{\partial^4 w(x,t)}{\partial x^4} + B \frac{\partial^3 u(x,t)}{\partial x^3} = \bar{\rho} \frac{\partial^2 w(x,t)}{\partial t^2}. \quad (2.24b)$$

The clamped-free boundary conditions of the PLSB ($x = 0, L_C$) can be shown as follows:

$$u|_{x=0} = 0, \quad \left[A \frac{\partial u(x,t)}{\partial x} - B \frac{\partial^2 w(x,t)}{\partial x^2} + N_p(t) \right]\bigg|_{x=L_c} = 0, \quad (2.25a)$$

$$w|_{x=0} = 0, \quad \left[B \frac{\partial^2 u(x,t)}{\partial x^2} - D \frac{\partial^3 w(x,t)}{\partial x^3} \right]\bigg|_{x=L_c} = 0, \quad (2.25b)$$

$$\frac{\partial w}{\partial x}\bigg|_{x=0} = 0, \quad \left[B \frac{\partial u(x,t)}{\partial x} - D \frac{\partial^2 w(x,t)}{\partial x^2} + M_p(t) \right]\bigg|_{x=L_c} = 0. \quad (2.25c)$$

As one may notice that there is no piezoelectric actuation term remains in Eqs. (2.24) for a similar reason to the above-mentioned case of PLSCB, which its piezoelectric induced control force and moment terms are equal to zero when taking partial derivative with respect to x-coordinate. The derived equations of motion of PLSB, Eq. (2.24), are the same as those non-piezo-electric straight composite beams by Vinson (2002). Note that the boundary conditions of the PLSB are different from those of non-piezoelectric straight composite beams due to the additional of the boundary piezoelectric induced control force and moment terms.

3. Solution methods

In this section, the DTFM by Yang and Tan (1992) is applied and extended to carry out the transfer function formulations of the PLSCB and PLSB models. This method will be used to solve for the natural frequencies, mode shapes and transfer functions of the cantilevered PLSCB and PLSB models. The natural frequencies of the cantilevered PLSCB and PLSB will be calculated by the DTFM and the Rayleigh–Ritz method.

Based on the DTFM, the governing equations of the cantilevered PLSCB and PLSB associated with its boundary conditions, Eqs. (2.22–2.25), are cast into the equivalent spatial state form and Laplace transformed with respect to time as follows:

$$\frac{d}{dx}\{\eta_k(x,s)\} = [F_k(s)]\eta_k(x,s) + P_k(s), \quad 0 \leqslant x \leqslant L_c, \quad (3.1)$$

where

$$k = \begin{cases} 1 & \text{for } PLSCB, \\ 2 & \text{for } PLSB, \end{cases}$$

$$F_1(s) = \begin{bmatrix} 0 & 0 & 0 & 1 & 0 & 0 \\ 0 & 0 & 1 & 0 & 0 & 0 \\ 0 & 0 & 0 & 0 & 1 & 0 \\ \frac{\bar{\rho}}{A}s^2 & 0 & -\frac{1}{R} & 0 & 0 & \frac{B}{A} \\ 0 & 0 & 0 & 0 & 0 & 1 \\ 0 & -\frac{\bar{\rho}}{\alpha}s^2 - \frac{A}{\alpha R^2} & 0 & \frac{B\bar{\rho}}{\alpha A}s^2 - \frac{A}{\alpha R} & \frac{B}{\alpha R} & 0 \end{bmatrix},$$

$$P_1(s) = \begin{bmatrix} 0 & 0 & 0 & 0 & 0 & \frac{-\bar{N}_p(s)}{\alpha R} \end{bmatrix}^T, \quad P_2(s) = [0]_{6 \times 1},$$

$$F_2(s) = \begin{bmatrix} 0 & 0 & 0 & 1 & 0 & 0 \\ 0 & 0 & 1 & 0 & 0 & 0 \\ 0 & 0 & 0 & 0 & 1 & 0 \\ \frac{\bar{\rho}}{A}s^2 & 0 & 0 & 0 & 0 & \frac{B}{A} \\ 0 & 0 & 0 & 0 & 0 & 1 \\ 0 & -\frac{\bar{\rho}}{\alpha}s^2 & 0 & \frac{B\bar{\rho}}{\alpha A}s^2 & 0 & 0 \end{bmatrix},$$

$$\alpha = D - \frac{B^2}{A},$$

$$\eta_k(x,s) = \begin{bmatrix} u & w & \frac{\partial w}{\partial x} & \frac{\partial u}{\partial x} & \frac{\partial^2 w}{\partial x^2} & \frac{\partial^3 w}{\partial x^3} \end{bmatrix}^T.$$

The boundary conditions, Eqs. (2.23) and (2.25), can also be written in terms of $\{\eta_k(x,s)\}$:

$$[M_k]\{\eta_k(0,s)\} + [N_k]\{\eta_k(L_c,s)\} = \{\gamma_k(s)\}, \quad (3.2)$$

$[M_k]$ and $[N_k]$ are 6×6 matrices and $\{\gamma_k(s)\}$ is a vector of boundary control piezoelectric induced strain force and moment

$$M_1 = \begin{bmatrix} 1 & 0 & 0 & 0 & 0 & 0 \\ 0 & 1 & 0 & 0 & 0 & 0 \\ 0 & 0 & 1 & 0 & 0 & 0 \\ 0 & 0 & 0 & 0 & 0 & 0 \\ 0 & 0 & 0 & 0 & 0 & 0 \\ 0 & 0 & 0 & 0 & 0 & 0 \end{bmatrix}, \quad N_1 = \begin{bmatrix} 0 & 0 & 0 & 0 & 0 & 0 \\ 0 & 0 & 0 & 0 & 0 & 0 \\ 0 & 0 & 0 & 0 & 0 & 0 \\ 0 & \frac{A}{R} & 0 & A & -B & 0 \\ \frac{B}{A}\rho s^2 & 0 & 0 & 0 & 0 & \frac{B^2}{A}-D \\ 0 & \frac{B}{R} & 0 & B & -D & 0 \end{bmatrix}, \quad \gamma_1 = \begin{bmatrix} 0 \\ 0 \\ 0 \\ -\bar{N}_p(s) \\ 0 \\ -\bar{M}_p(s) \end{bmatrix},$$

$$M_2 = \begin{bmatrix} 1 & 0 & 0 & 0 & 0 & 0 \\ 0 & 1 & 0 & 0 & 0 & 0 \\ 0 & 0 & 1 & 0 & 0 & 0 \\ 0 & 0 & 0 & 0 & 0 & 0 \\ 0 & 0 & 0 & 0 & 0 & 0 \\ 0 & 0 & 0 & 0 & 0 & 0 \end{bmatrix}, \quad N_2 = \begin{bmatrix} 0 & 0 & 0 & 0 & 0 & 0 \\ 0 & 0 & 0 & 0 & 0 & 0 \\ 0 & 0 & 0 & 0 & 0 & 0 \\ 0 & 0 & 0 & A & -B & 0 \\ \frac{B}{A}\rho s^2 & 0 & 0 & 0 & 0 & \frac{B^2}{A}-D \\ 0 & 0 & 0 & B & -D & 0 \end{bmatrix}, \quad \gamma_2 = \begin{bmatrix} 0 \\ 0 \\ 0 \\ -\bar{N}_p(s) \\ 0 \\ -\bar{M}_p(s) \end{bmatrix}.$$

Here, $\bar{N}_p(s)$ and $\bar{M}_p(s)$ are the Laplace transforms of $N_p(t)$ and $M_p(t)$, respectively.

Write the solution of Eq. (3.1) by assuming no external or internal input of piezoelectric induced strain force or moment as

$$\eta_k(x,s) = e^{[F_k(s)]x}\eta_k(0,s), \quad (3.3)$$

where $e^{F_k(s)x}$ is the fundamental matrix. Substituting Eq. (3.3) into the boundary conditions, Eq. (3.2), gives the homogeneous equation (assuming no piezoelectric induced strain force or moment)

$$([M_k] + [N_k]e^{[F_k(s)]}L_c)\eta_k(0,s) = 0. \quad (3.4)$$

The characteristic equations of the PLSCB and PLSB, Eq. (3.4), are

$$\Delta(\omega) \equiv \det\left([M_k] + [N_k]e^{[F_k(s)]}L_c\right) = 0, \quad (3.5)$$

where $\Delta(\omega)$ is a transcendental function with an infinite number of roots. The characteristic equation can be accurately and easily solved by standard root-searching techniques. Its roots are of the form

$$s = j\omega_n, \quad j = \sqrt{-1}, \quad n = 1, 2, \ldots, \quad (3.6)$$

where ω_n are the nth natural frequencies of the system. The mode shapes corresponding to ω_n can be obtained by solving Eq. (3.4) for a non-zero $\eta_k(0,s)$ at $s = j\omega_n$ and substituting the result into Eq. (3.3).

The solution of the state-space equations (3.1) and (3.2) is in exact and closed form (Yang and Tan, 1992) can be formulated as follows:

$$\eta_k(x,s) = \int_0^{L_c} G_k(x,\zeta,s)P_k(\zeta,s)d\zeta + H_k(x,s)\gamma_k(s), \quad x \in (0,L_c),$$
(3.7)

where

$$k = \begin{cases} 1 & \text{for } PLSCB, \\ 2 & \text{for } PLSB, \end{cases}$$

$$G_k(x,\zeta,s) = \begin{cases} e^{F_k(s)x}(M_k + N_k e^{F_k(s)L_c})^{-1}M_k e^{-F_k(s)\zeta}, & \zeta \leqslant x, \\ -e^{F_k(s)x}(M_k + N_k e^{F_k(s)L_c})^{-1}N_k e^{F_k(s)(L_c-\zeta)}, & \zeta \geqslant x, \end{cases}$$

$$= \begin{bmatrix} g_{k11}(x,\zeta,s) & \dots & g_{k1r}(x,\zeta,s) \\ \vdots & & \vdots \\ g_{kr1}(x,\zeta,s) & \dots & g_{krr}(x,\zeta,s) \end{bmatrix}_{r \times r},$$
(3.8a)

$$H_k(x,s) = e^{F_k(s)x}(M_k + N_k e^{F_k(s)L_c})^{-1}$$

$$= \begin{bmatrix} h_{k11}(x,s) & \dots & h_{k1r}(x,s) \\ \vdots & & \vdots \\ h_{kr1}(x,s) & \dots & h_{krr}(x,s) \end{bmatrix}_{r \times r}.$$
(3.8b)

The matrices $G_k(x,\zeta,s)$ and $H_k(x,s)$ are called the distributed transfer functions of the PLSCB or PLSB.

The Rayleigh–Ritz (Meirovitch, 2003) method requires minimization of the Lagrangian energy functionals, namely, the potential and kinetic energies of the continuous beams, in order to compute for approximate natural frequencies. The Lagrangian, $L = T - \Pi$, is then minimized by taking its derivatives with respect to the undetermined coefficients of the displacement fields and making them equal to zero, shown as follows:

$$\frac{\partial L}{\partial a_i} = \frac{\partial(T - \Pi_1 - \Pi_2 - \Pi_3)}{\partial a_i} = 0, \quad i = 1, 2, \dots, N,$$

$$\frac{\partial L}{\partial b_i} = \frac{\partial(T - \Pi_1 - \Pi_2 - \Pi_3)}{\partial b_i} = 0, \quad i = 1, 2, \dots, N.$$
(3.9)

This yields equations that can be written in a matrix form and give the natural frequencies as follows:

$$([K] - \omega^2[M])(\gamma) = \left(\begin{bmatrix} k_{ua} & k_{ub} \\ k_{wa} & k_{wb} \end{bmatrix} - \omega^2 \begin{bmatrix} m_{ua} & m_{ub} \\ m_{wa} & m_{wb} \end{bmatrix} \right) \begin{pmatrix} a_N \\ b_N \end{pmatrix} = 0.$$
(3.10)

Further details of the Rayleigh–Ritz method and its definitions used for computing the approximate natural frequencies of the PLSCB and PLSB models are shown in Appendix A.

4. Numerical examples and discussion

The physical parameters of the PLSCB and PLSB are tabulated in Table 2. In free vibration analysis, the first five natural frequencies of the cantilevered PLSCB and PLSB, as listed in Table 3, are computed with the DTFM and the Rayleigh–Ritz approximation ($N = 6$ and $N = 10$). The convergence is good for the first two modes except for higher modes of all cases using the Rayleigh–Ritz method ($N = 6$). For the first four modes of the PLSCB with large radii of curvature, $R = 1$ and $R = \infty$, respectively, both the DTFM prediction and Rayleigh–Ritz method with higher order, $N = 10$ have yielded the exact same values. However, for the 5th mode, the DTFM prediction has a deviation of 10% from the Rayleigh–Ritz method with higher order, $N = 10$.

As for the first four modes of the PLSB with small radius of curvature, $R = 0.01$, both the DTFM prediction and Rayleigh–Ritz approximation with higher order, $N = 10$ have yielded exact same values except for the 4th mode, which the DTFM prediction has a deviation of 8.7% from the Rayleigh–Ritz method with higher order, $N = 10$.

From the above analysis, one can observe that by increasing the order of the Rayleigh–Ritz approximation, the lowest newly computed natural frequencies decrease relative to the corresponding previously computed natural frequencies, or at least they do not increase.

The most important observation made about these results is the strong effect of the bending–stretching coupling due to unsymmetrical lamination. The stretching–bending coupling due to curvature has a considerable effect on the frequency parameters. Increasing the radius of curvature of the PLSCB has its largest effect on the natural frequencies. The Rayleigh–
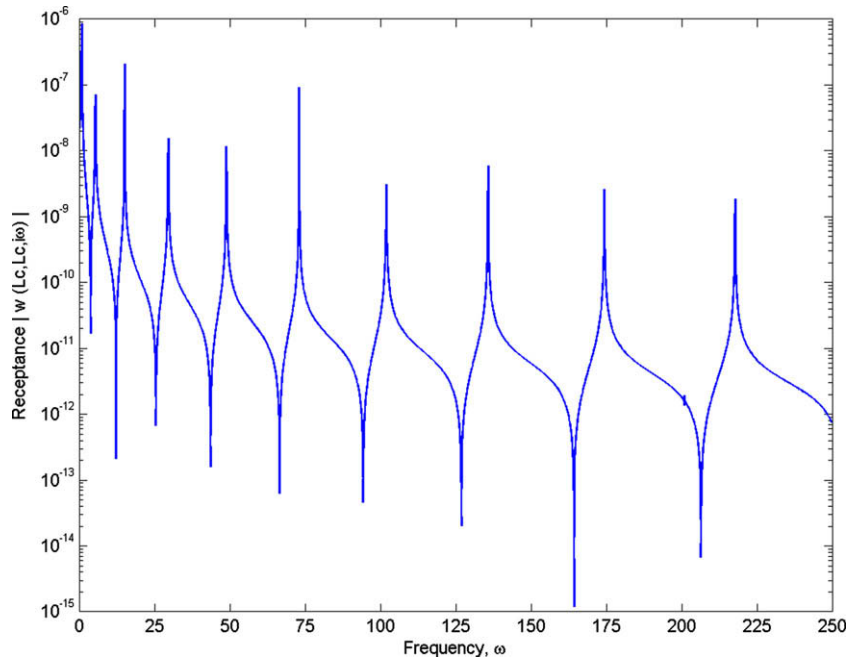
Table 2
Material properties of the PLSCB and PLSB.

Material property	PZT 3195 HD	LaRC-SI	302 Stainless steel
Young's modulii (N/m^2), Y	6.7×10^{10}	4.0×10^9	2.62×10^9
Piezoelectric strain constant (C/N), d_{31}	-190×10^{-12}	–	–
Width (m), b	5.97×10^{-3}	5.97×10^{-3}	5.97×10^{-3}
Length (m), L_C	3.26×10^{-2}	3.26×10^{-2}	3.26×10^{-2}
Thickness (m)	2.03×10^{-4}	2.54×10^{-5}	1.52×10^{-4}
Number of layers	1	1	1

Table 3
Natural frequencies of the PLSCB and PLSB.

Mode no.	DTFM			Rayleigh–Ritz				
	PLSCB		PLSB	PLSCB				PLSB
	$R = 0.01$	$R = 1$	$R = \infty$	$R = 0.01$		$R = 1$		$R = \infty$
				$N = 6$	$N = 10$	$N = 6$	$N = 10$	$N = 10$
1	0.45	0.85	0.85	0.46	0.46	0.86	0.86	0.86
2	3.15	5.39	5.40	3.22	3.16	5.39	5.40	5.40
3	11.3	15.09	15.10	22.90	11.4	15.52	15.10	15.10
4	25.1	29.59	29.60	129.7	27.5	31.49	29.65	29.65
5	43.9	48.80	48.90	573.4	65.1	137.7	54.4	54.4

Fig. 3. The receptance $|W_0(L_c, L_c, i\omega)|$ of the PLSCB; $R = 1$.
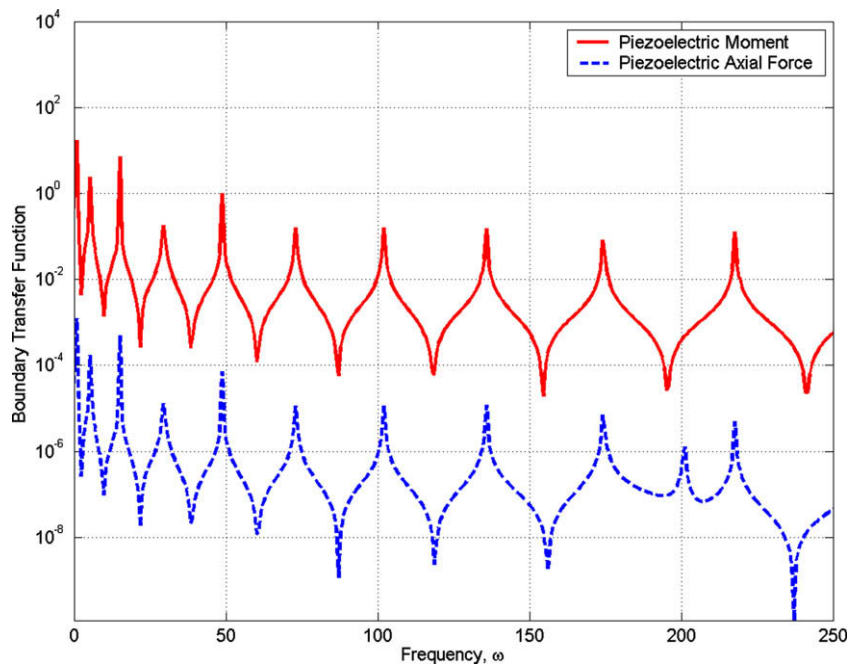

Fig. 4. Effect of the inhomogeneous boundary conditions on PLSCB; $R = 1$.

Ritz method requires appropriate and higher degrees of the polynomial displacement functions, which has been done by Qatu (1992) and Qatu and Elsharkawy (1993) to improve the convergence in obtaining the natural frequencies of the non-piezoelectric/piezoelectric laminated curved beams with the compensation of computation memory and time. According to Rayleigh–Ritz principle (Meirovitch, 2003), the approximate natural frequencies represented upper bounds for the actual natural frequencies. Thus, one can observe that the computation of the natural frequencies by the DTFM is more accurate than

the Rayleigh–Ritz method, since the natural frequencies calculated by the DTFM are less than those by the Rayleigh–Ritz method.

Consider the first term of Eq. (3.7) for the formulation of receptance transfer function of the PLSCB, $\bar{w}(L_c, j\omega)/\overline{N}_p(j\omega) = \alpha R \times |g_{126}(x = L_c, \zeta = L_c, j\omega)|$, which defines the colocated piezoelectric induced force control acted at $\zeta = L_c$ of the beam to the output beam vibration observed at $x = L_c$, is shown in Fig. 3. Ten resonance peaks of the cantilevered PLSCB are shown. It is observed that the frequency shift becomes larger for higher modes.
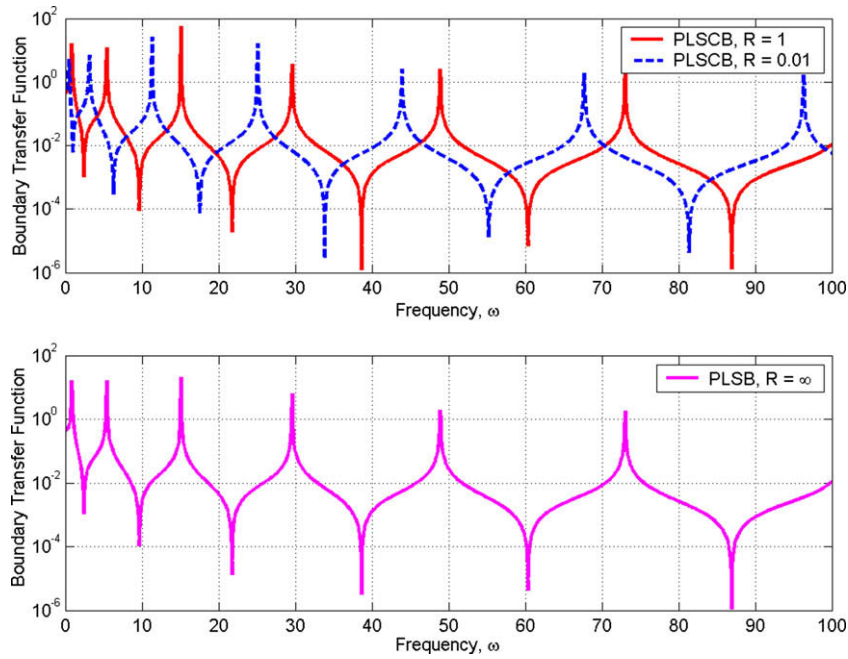
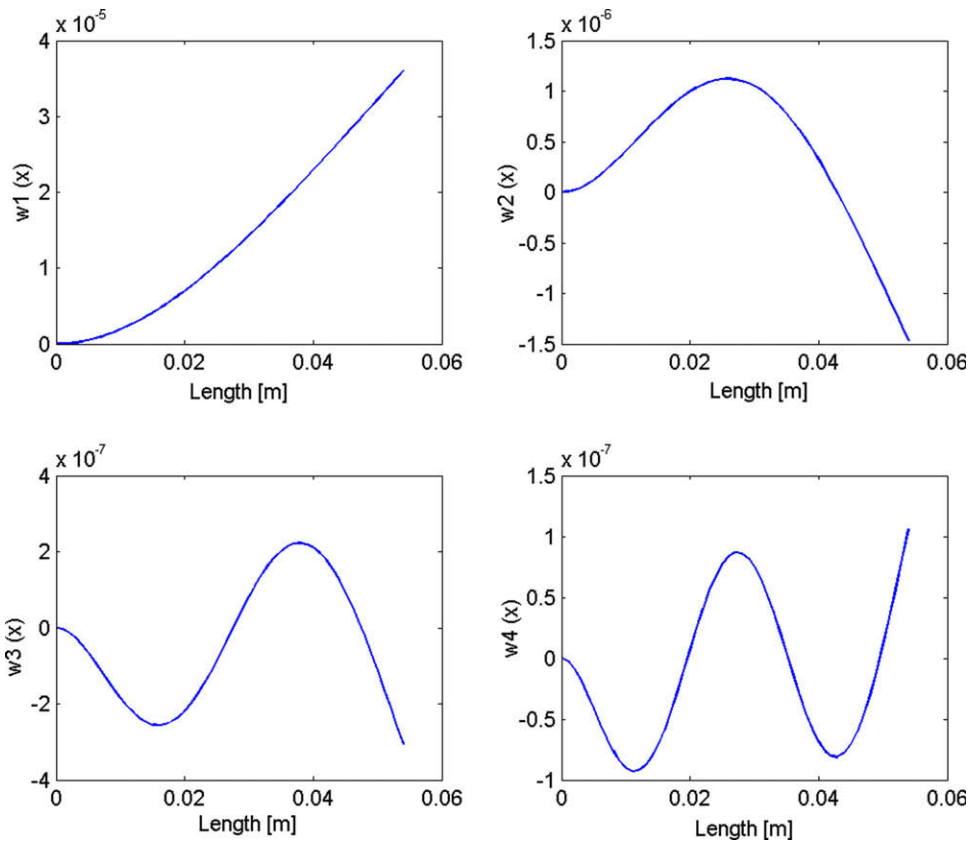Fig. 5. Effect of the inhomogeneous boundary conditions with varies of radius of curvature, R.

Fig. 6. First four mode shapes of clamped-free PLSCB; R = 1.

Consider the second term of Eq. (3.7) for the formulation of boundary control transfer functions of the PLSCB, $\bar{w}(L_c, j\omega)/\overline{N}_p(j\omega) = |h_{124}|$ and $\bar{w}(L_c, j\omega)/\overline{M}_p(j\omega) = |h_{126}|$, which define piezoelectric induced force and moment acted at the right end of the beam to the beam vibration, respectively, are shown in Fig. 4. As one can notice that the inhomogeneity of the boundary

conditions does not have any effects on the natural frequencies or system spectrum due to the both receptance of the system, $G_k(x, \zeta, s)$ and boundary transfer function, $H_k(x, s)$ have the same characteristic equations, as shown in Eq. (3.8).

Fig. 5 shows the effects of increasing the radius of curvature on the resonant frequencies of the cantilevered PLSCB and PLSB. As
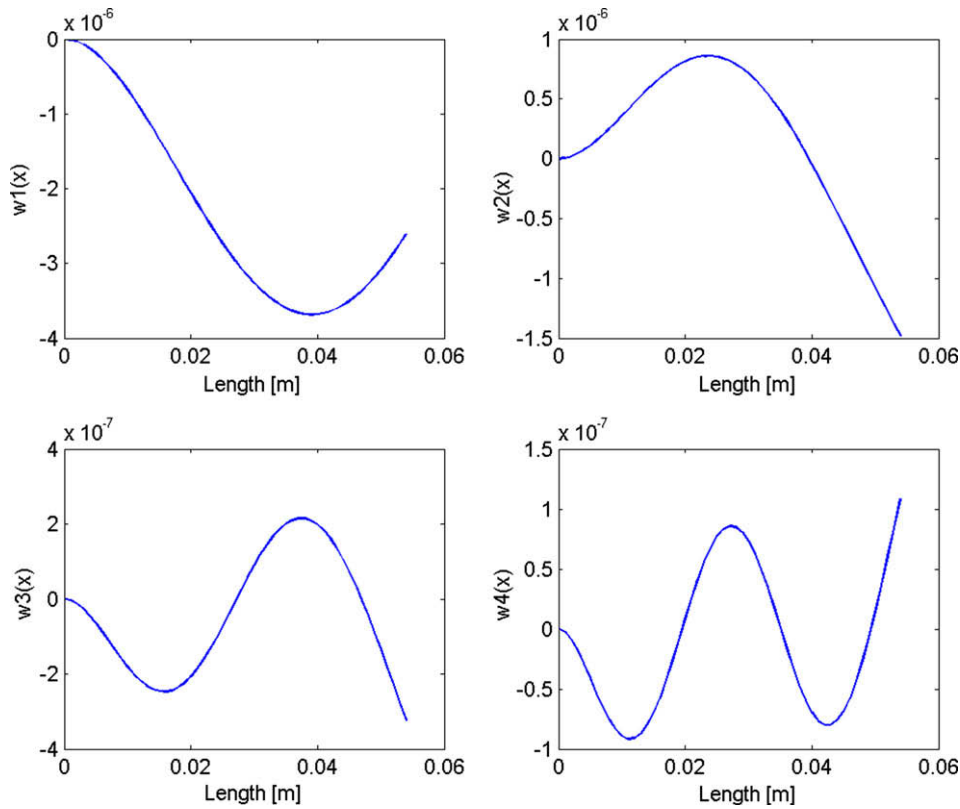
Fig. 7. Mode shapes of clamped-elastically constrained PLSCB; k = 100 N/m; R = 1.

the radius of curvature of the PLSCB increases, its resonant frequencies tend to shift to the same values as those of the PLSB.

Fig. 6 shows four vibration modes of the cantilevered PLSCB. These vibration modes are obtained by solving Eq. (3.3), in which its non-zero $\eta_1(0, s)$ at $s = j\omega_n$, $n = 1, 2, 3, 4$ can be found from Eq. (3.4). This demonstrates the DTFM method is very convenient to compute the vibration modes of the PLSCB that does not require any eigensolutions.

Fig. 7 shows four vibration modes of a clamped-elastically constrained ($k_{spring} = 100$ N/m) PLSCB. These vibration modes can be obtained by simply adding the spring constant term, k_{spring} to the (5, 2) element of matrix N_1 of Eq. (3.2). The modified boundary matrix N_1 of the clamped-elastically constrained PLSCB can be formulated as follows:

$$N_1 = \begin{bmatrix} 0 & 0 & 0 & 0 & 0 & 0 \\ 0 & 0 & 0 & 0 & 0 & 0 \\ 0 & 0 & 0 & 0 & 0 & 0 \\ 0 & \frac{A}{R} & 0 & A & -B & 0 \\ \frac{B}{A}\rho s^2 & k_{spring} & 0 & 0 & 0 & \frac{B^2}{A} - D \\ 0 & \frac{B}{R} & 0 & B & -D & 0 \end{bmatrix}.$$

This example demonstrates that the DTFM method is also very convenient to compute the mode shapes of the composite curved beams with arbitrary inhomogeneity boundary conditions.

5. Conclusions

The generic model of PLSCB has been derived, including the computation of the natural frequencies, mode shapes and the transfer functions using the DTFM. By setting the radius of curvature of the proposed model to infinity, the PLSB model can be

obtained. The DTFM is extended to solve for the natural frequencies and mode shapes of the cantilevered PLSCB and PLSB models in exact and closed-form solution without using truncated series of particular comparison or admissible functions, and therefore is capable of precisely modeling of abrupt changes in system properties with arbitrary inhomogeneity boundary conditions. Furthermore, this method does not require knowledge of the system eigensolutions. Compared to Rayleigh–Ritz method, the DTFM has the capability of providing exact and closed-form solution for vibration analysis of the composite beams with arbitrary boundary conditions and physical insight behavior of the continuous structure. The proposed model and the solution method can also be generalized to the vibration analysis of non-piezoelectric composite beams with arbitrary boundary conditions.

Appendix A

Define $\chi = \begin{cases} 1 & \text{for } PLSCB, \\ 0 & \text{for } PLSB, \end{cases}$

$$\Pi_1 = \frac{1}{2} \int_0^L \left[A \left(\left(\frac{\partial u}{\partial x} \right)^2 + \frac{2}{R} \chi w \frac{\partial u}{\partial x} + \frac{1}{R^2} \chi w^2 \right) \right] dx,$$

$$\Pi_2 = \frac{1}{2} \int_0^L \left[D \left(\frac{\partial^2 w}{\partial x^2} \right)^2 \right] dx, \qquad (A.1)$$

$$\Pi_3 = \frac{1}{2} \int_0^L \left[-2B \left(\frac{\partial u}{\partial x} + \chi \frac{w}{R} \right) \frac{\partial^2 w}{\partial x^2} \right] dx,$$

$$u(x) = \sum_{j=1}^N a_j \varphi_j, \quad w(x) = \sum_{j=1}^N b_j \phi_j,$$

$$\gamma = [a_1, a_2, \ldots, a_N, b_1, b_2, \ldots, b_N], \qquad (A.2)$$

$$0 = \frac{\partial T}{\partial a_i} = \omega^2 \bar{\rho} \int_0^L \left[\varphi_i \left(\sum_{j=1}^N a_j \varphi_j \right) \right] dx,$$

$$0 = \frac{\partial T}{\partial b_i} = \omega^2 \bar{\rho} \int_0^L \left[\phi_i \left(\sum_{j=1}^N b_j \phi_j \right) \right] dx, \tag{A.3}$$

$$0 = \frac{\partial \Pi_1}{\partial a_i} = \int_0^L \left[A \frac{d\varphi_i}{dx} \left(\sum_{j=1}^N a_j \frac{d\varphi_j}{dx} \right) + \frac{A}{R} \chi \frac{d\varphi_i}{dx} \left(\sum_{j=1}^N b_j \frac{d\phi_j}{dx} \right) \right] dx,$$

$$0 = \frac{\partial \Pi_1}{\partial b_i} = \int_0^L \left[\frac{A}{R} \chi \phi_i \left(\sum_{j=1}^N a_j \frac{d\varphi_j}{dx} \right) + \frac{A}{R^2} \chi \phi_i \left(\sum_{j=1}^N b_j \phi_j \right) \right] dx,$$

$$0 = \frac{\partial \Pi_2}{\partial a_i},$$

$$0 = \frac{\partial \Pi_2}{\partial b_i} = \int_0^L \left[D \frac{d^2 \phi_i}{dx^2} \left(\sum_{j=1}^N b_j \frac{d^2 \phi_j}{dx^2} \right) \right] dx,$$

$$0 = \frac{\partial \Pi_3}{\partial a_i} = - \int_0^L \left[B \frac{d\varphi_i}{dx} \left(\sum_{j=1}^N b_j \frac{d^2 \phi_j}{dx^2} \right) \right] dx,$$

$$0 = \frac{\partial \Pi_3}{\partial b_i} = - \int_0^L \left[B \frac{d^2 \phi_i}{dx^2} \left(\sum_{j=1}^N a_j \frac{d\varphi_j}{dx} \right) + \frac{B}{R} \chi \phi_i \left(\sum_{j=1}^N b_j \frac{d^2 \phi_j}{dx^2} \right) \right] dx, \tag{A.4}$$

$$m_{ua} = \bar{\rho} \int_0^L [\varphi_i \varphi_j] dx, \quad m_{wb} = \bar{\rho} \int_0^L [\phi_i \phi_j] dx,$$

$$m_{ub} = \begin{bmatrix} 0 & \cdots & 0 \\ \vdots & \ddots & \vdots \\ 0 & \cdots & 0 \end{bmatrix}_{N \times N}, \quad m_{wa} = \begin{bmatrix} 0 & \cdots & 0 \\ \vdots & \ddots & \vdots \\ 0 & \cdots & 0 \end{bmatrix}_{N \times N}, \tag{A.5}$$

$$k_{ua} = A \int_0^L \left[\frac{d\varphi_i}{dx} \frac{d\varphi_j}{dx} \right] dx,$$

$$k_{wb} = \int_0^L \left[\frac{A}{R^2} \chi \phi_i \phi_j + D \frac{d^2 \phi_i}{dx^2} \frac{d^2 \phi_j}{dx^2} - \frac{B}{R} \chi \left(\phi_i \frac{d^2 \phi_j}{dx^2} \right) \right] dx,$$

$$k_{ub} = \int_0^L \left[\frac{A}{R} \chi \frac{d\varphi_i}{dx} \phi_j - B \frac{d\varphi_i}{dx} \frac{d^2 \phi_j}{dx^2} \right] dx, \tag{A.6}$$

$$k_{wa} = \int_0^L \left[\frac{A}{R} \chi \phi_i \frac{d\varphi_j}{dx} - B \frac{d^2 \phi_i}{dx^2} \frac{d\varphi_j}{dx} \right] dx,$$

where φ_j and ϕ_j are the chosen polynomial shape functions that satisfy only the essential boundary conditions.

References

Archer, R.R., 1960. Small vibrations of thin incomplete circular rings. International Journal of Mechanical Science 1, 45–56.

Auciello, N.M., De Rosa, M.A., 1993. Free vibrations of circular arches. Journal of Sound and Vibration 176, 433–458.

Balakrishnan, S., Niezrecki, C., 2001. Power characterization of THUNDER actuators as underwater propulsors, in: Proceedings of SPIE, vol. 4327, pp. 88–98.

Buckens, F., 1950. Influence of the relative radial thickness of a ring on its natural frequencies. Journal of the Acoustical Society of America 22, 437–443.

Chidamparam, P., Leissa, A.W., 1995. Influence of centerline extensibility on the in-plane free vibrations of loaded circular arches. Journal of Sound and Vibration 183, 779–795.

Clark, W.W., Smith, R., Janes, K., Winkler, J., Mulcahy, M., 2000. Development of a piezoelectrically actuated cell stretching device. In: Proceedings of SPIE, vol. 3991, pp. 294–301.

Crawley, E.F., de Luis, J., 1987. Use of piezoelectric actuators as elements of intelligent structures. Journal of AIAA 25, 1385–1676.

Damjanovic, D., Newnham, R.E., 1992. Electrostrictive and piezoelectric materials for actuators applications. Journal of Intelligent Material Systems and Structures 3, 190–208.

Den Hartog, J.P., 1928. The lowest natural frequency of circular arcs. Philosophical Magazine, Ser. 7 (5), 400–408.

Dym, C.L., 1980. On the vibration of thin circular rings. Journal of Sound and Vibration 70, 585–588.

Granger, R., Washington, G., Kwak, S.-K., 2000. Modeling and control of a singly curved active aperture antenna using curved piezoceramic actuators. Journal of Intelligent Material Systems and Structures 11, 225–233.

Hammoud, A.S., Archer, R.R., 1963. On the free vibration of complete and incomplete circular rings. Developments in Mechanics 2, 489–524.

IEEE, 1998. IEEE standard on piezoelectricity. ANSI/IEEE Standard, 176-1987, New York.

Irie, T., Yamada, G., Tanaka, K., 1983. Natural frequencies of in-plane vibration of arcs. Journal of Applied Mechanics 50, 449–452.

Larson, P.H., Vinson, J.R., 1993. The use of piezoelectric materials in curved beams and rings. Adaptive Structures and Material Systems 35, 277–285.

Laura, P.A.A., Maurizi, M.J., 1987. Recent research on vibrations arch-type structures. Shock and Vibration Digest 19, 6–9.

Love, A.E.H., 1944. A Treatise on the Mathematical Theory of Elasticity. Dover, New York.

Meirovitch, L., 2003. Fundamentals of Vibrations. McGraw-Hill, New York.

Mitchell, L.A., Gu, H., Chattopadhyay, A., 1997. Improved modeling of C-Block actuators. In: Proceedings of SPIE, vol. 3041, pp. 470–481.

Moskalik, A.J., Brei, D., 1997. Quasi-static behavior of individual C-block piezoelectric actuators. Journal of Intelligent Material Systems and Structures 8, 571–587.

Moskalik, A.J., Brei, D., 1999. Force-deflection behavior of piezoelectric C-block actuators arrays. Smart Materials & Structures 8, 531–543.

Mossi, K.M., Bishop, R.P., Smith, R.C., Banks, H.T., 1999. Evaluation criteria for THUNDER actuators. In: Proceedings of SPIE, vol. 3667, pp. 738–743.

Nelson, F.C., 1962. In-plane vibration of a simply supported circular ring segment. International Journal of Mechanical Science 4, 517–527.

Ounaies, Z., Mossi, K., Smith, R., Bernd, J., 2001. Low-field and high-field characterization of THUNDER actuators. In: Proceedings of SPIE, vol. 4333, pp. 399–407.

Qatu, M.S., 1992. In-plane vibration of slightly curved laminated composite beams. Journal of Sound and Vibration 159, 327–338.

Qatu, M.S., 1993. Theories and analysis of thin and moderately thick laminated composite curved beams. International Journal of Solids and Structures 30, 2743–2756.

Qatu, M.S., Elsharkawy, A., 1993. Vibrations of laminated composite arches with deep curvature and arbitrary boundaries. Computers and Structures 47, 305–311.

Qatu, M.S., 2004. Vibration of Laminated Shells and Plates. Elsevier, Amsterdam.

Rao, S.S., Sundararajan, V., 1969. In-plane flexural vibration of circular rings. Journal of Applied Mechanics 36, 620–625.

Seidel, B.S., Erdelyi, E.A., 1964. On the vibration of a thick ring in its own plane. Journal of Engineering for Industry 86, 240–244.

Schaffer, J., Rizen, M., L'Italien, G.J., Benbrahim, A., Megerman, J., Gerstenfeld, L.C., Gray, M.L., 1994. Device for the application of a dynamic biaxially uniform and isotropic strain to a flexible cell culture membrane. Journal of Orthopaedic Research 12, 709–719.

Shakeri, C., Bordonaro, C.M., Noori, M.N., Champagne, R., 1999. Experimental study of THUNDER: a new generation of piezoelectric actuators. In: Proceedings of SPIE, vol. 3675, pp. 63–71.

Susanto, K., Yang, B., 2007. Modeling and design of a piezoelectric forceps actuator for meso/micro grasping. ASME Journal of Medical Devices 1, 30–37.

Susanto, K., Yang, B., 2004. Data glove-based fuzzy control of piezoelectric forceps actuator. In: Proceedings of SPIE, vol. 5390, pp. 388–339.

Susanto, K., 2008. Piezoelectric forceps actuator: theory and experiments. Review of Scientific Instruments 79, 115106–115106-5.

Tanaka, S., 1999. A new mechanical stimulator for cultured bone cells using piezoelectric actuator. Journal of Biomechanics 32, 427–430.

Veletsos, A.S., Austin, W.J., Pereira, C.A.L., Wung, S., 1972. Free in-plane vibration of circular arches. Journal of Engineering Mechanics 98, 311–329.

Vinson, J.R., 2002. The Behavior of Structures Composed of Composite Materials. Kluwer Academic Publishers, Dordrecht.

Washington, G., 1996. Smart aperture antennas. Smart Materials & Structures 5, 801–805.

Yoon, K.J., Shin, S., Kim, J., Park, H.C., Kwak, M.K., 2000. Development of lightweight THUNDER with fiber composite layers. In: Proceedings of SPIE, vol. 3992, pp. 57–64.

Yang, B., Tan, C.A., 1992. Transfer functions of one-dimensional distributed parameter systems. ASME Journal of Applied Mechanics 59, 1009–1014.